Journal of Medicinal Chemistry

pubs.acs.org/jmc Article

Convenient Retinoid X Receptor Binding Assay Based on Fluorescence Change of the Antagonist NEt-C343

Kayo Yukawa-Takamatsu, Yifei Wang, Masaki Watanabe, Yuta Takamura, Michiko Fujihara, Mariko Nakamura-Nakayama, Shoya Yamada, Shota Kikuzawa, Makoto Makishima, Mayu Kawasaki, Sohei Ito, Shogo Nakano, and Hiroki Kakuta*

Cite This: J. Med. Chem. 2021, 64, 861−870 Read Online

ACCESS | Metrics & More | Article Recommendations | Supporting Information

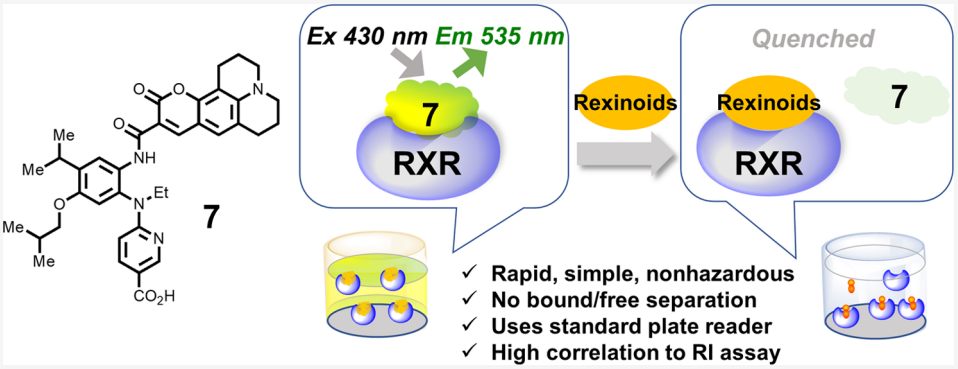

ABSTRACT: Retinoid X receptor (RXR) modulators (rexinoids) are considered to have therapeutic potential for multiple diseases, such as Alzheimer's disease and Parkinson's disease. To overcome various disadvantages of prior screening methods, we previously developed an RXR binding assay using a fluorescent RXR ligand, CU-6PMN (**4**). However, this ligand binds not only at the ligand-binding domain (LBD) but also at the dimer−dimer interface of hRXRα. Here, we present a new fluorescent RXR antagonist 6-[*N*-ethyl-*N*-(5-isobutoxy-4-isopropyl-2-(11-oxo-2,3,6,7-tetrahydro-1*H*,5*H*,11*H*-pyrano[2,3-*f*]pyrido[3,2,1-*ij*]quinoline-10-carboxamido)phenyl)amino]nicotinic acid (NEt-C343, **7**), which emits strong fluorescence only when bound to the RXR-LBD. It allows us to perform a rapid, simple, and nonhazardous binding assay that does not require bound/free separation and uses a standard plate reader. The obtained *K*i values of known compounds were correlated with the *K*i values obtained using the standard [^{3}H]9*cis*-retinoic acid assay. This assay should be useful for drug discovery as well as for research on endocrine disruptors, functional foods, and natural products.

INTRODUCTION

Bexarotene (**1**) (Figure 1), which is a retinoid X receptor (RXR) agonist, was initially approved to treat cutaneous T-cell lymphoma (CTCL). Recently, in the phase II clinical trial in tamoxifen-resistant breast cancer patients, **1** has shown efficacy in about 20% of patients with tolerable toxicity in combination with tamoxifen.[1] **1** has been researched for drug repositioning in not only cancer but also other diseases. For instance, it is reported that **1** shows a reduction of amyloid beta in the brain of patients with mild to moderate Alzheimer's disease in a small clinical trial.[2] **1** also restored behavioral function in a rat model of Parkinson's disease.[3] This variety of biological activities is thought to be attributable to RXR modulation.

RXR is one of the 48 nuclear receptors in humans, including retinoic acid receptors (RARs), vitamin D receptor (VDR), and thyroid hormone receptors (TRs).[4,5] RXR serves as a heterodimeric partner with various other nuclear receptors, such as peroxisome proliferator-responsive receptors (PPARs), liver X receptors (LXRs), and nuclear receptor related 1 protein (Nurr1). Therefore, RXR modulators (also known as rexinoids[6]) are involved in a wide range of cellular processes, including cell differentiation and proliferation, by regulating various transcriptional activities in a heterodimer-dependent manner. There are three RXR subtypes, RXRα, RXRβ, and RXRγ,[7] and all of them are thought to have comparable cellular activities. Because of their important role in NR function, at least one RXR subtype is expressed in all cells, and the pattern of expression of the three subtypes differs throughout the body.[5,7] Subtype-selective RXR ligands have been investigated,

Received: October 31, 2020
Published: December 30, 2020

https://dx.doi.org/10.1021/acs.jmedchem.0c01883
J. Med. Chem. 2021, 64, 861−870

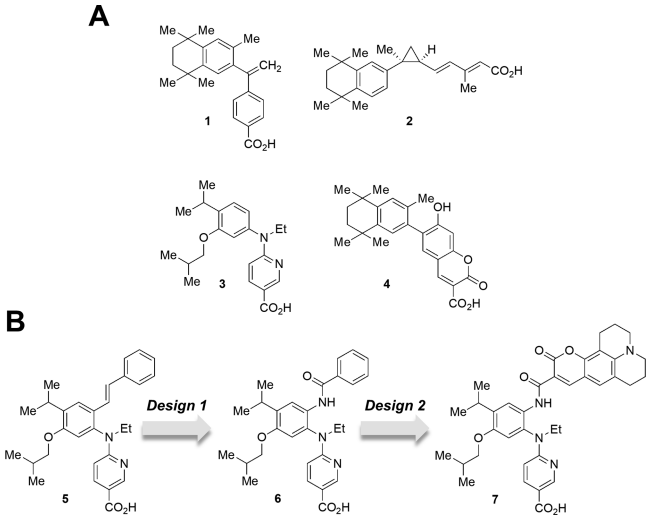

Figure 1. Chemical structures of **1**–**7** (A) and molecular design strategy from **5** (B).

but compounds with high specificity have not yet been discovered.[8,9]

Due to the various bioactivities arising from the diversity of RXR partners, rexinoids have been proposed as potential therapeutics for neurovegetative states, inflammatory disease, breast cancer, and metabolic disease.[10,11] For example, IRX4204 (**2**) (Figure 1), which activates RXR/Nurr1 heterodimers, improved behavioral function in a Parkinson's disease rat model and humans.[12] NEt-3IB (**3**) was reported to reduce blood glucose in a mouse model of diabetes.[13] However, the therapeutic potential of RXR ligands in humans remains to be explored due to the lack of safe RXR ligands with high subtype selectivity and low lipophilicity.[5] Therefore, there is great interest in efficient screening assays not only to potentially aid repositioning of existing drugs but also to discover new RXR modulators.

Reporter gene assays and time-resolved fluorescence resonance energy transfer (TR-FRET) assays are widely used as screening methods for the identification of rexinoids, besides the standard radioisotope method using [^{3}H]9-*cis*-retinoic acid ([^{3}H]9*cis*-RA).[14,15] These assays can easily measure the transcriptional activity of RXR. On the other hand, the reporter gene assay requires 3–4 days, the TR-FRET assay requires special equipment, and the [^{3}H]9*cis*-RA assay also requires special precautions.[14] Thus, there is a great need for a screening method that can detect rexinoids quickly using a standard plate reader, as is currently being done for RAR.[15] We have already applied a fluorescent rexinoid (**4**, CU-6PMN) for this purpose,[14] developing a rapid and nonhazardous assay method without the need for bound-free (B/F) separation. However, this suffers from the drawback that **4** binds not only at the ligand-binding domain (LBD) but also at the dimer–dimer interface of hRXRα, and we found that the interaction with the dimer–dimer interface induced a conformational change of the LBD, leading to a 1.5-fold increase of [^{3}H]9*cis*-RA binding. Consequently, it is not straightforward to compare the results obtained with the two assays. Therefore, in the present work, we aimed to design and synthesize a new fluorescent RXR ligand and employ it to develop a rapid, simple, and nonhazardous screening method that can potentially replace the [^{3}H]9*cis*-RA assay.

RESULTS AND DISCUSSION

Figure 1B shows the molecular design of the novel fluorescent RXR ligands synthesized here. NEt-SB (**5**), an RXR antagonist, shares the same skeleton as **3**, but with a stilbene motif.[16] Since the stilbene skeleton has a fluorescent character, we examined its fluorescence properties in detail.[17] However, **5** is unsuitable for the RXR ligand-binding assay because of its low fluorescence intensity and inappropriate fluorescence wavelength. Therefore, we designed NEt-BA (**6**) by replacing the stilbene with a benzanilide structure, its bioisostere. Moreover, NEt-C343 (**7**) was designed by the introduction of a fluorophore, coumarin 343 (**10**) (Scheme 1). We selected **10**

Scheme 1. Synthesis of (A) 10 and (B) 6 and 7[a]

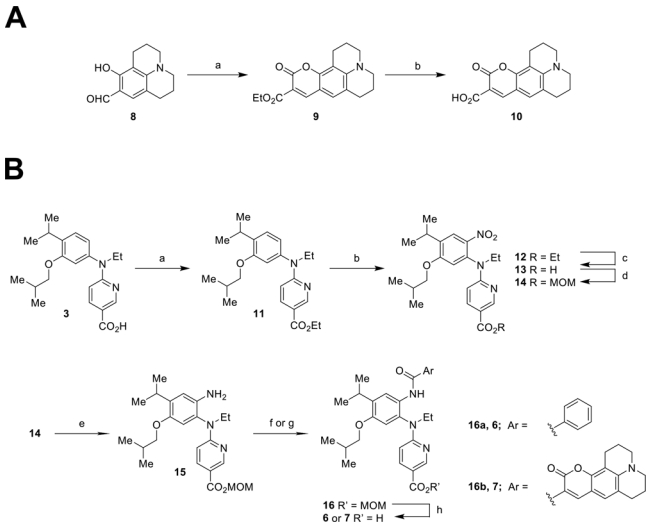

[a]Reagents and conditions: (A) (a) diethyl malonate, piperidine, 30 °C, 3 h, 43%. (b) (1) conc. HCl, r.t., 20 h; (2) 28% NH_3aq, 59%. (B) (a) EtOH, H_2SO_4, reflux, 21 h, q.y. (b) HNO_3, Ac_2O, r.t., 0.5 h, 75%. (c) 2 N NaOHaq, EtOH, 80 °C, 1 h, 85%. (d) MOMCl, TEA, DMF, 0 °C, 1 h, q.y. (e) H_2, Pd/C, EtOH, r.t., 3 h, 81%. (f) Benzoyl chloride, DIEPA, CH_2Cl_2, r.t., 17 h, q.y. (g) **10**, EDCI·HCl, HOBt·H_2O, DMF, r.t., 10 h, q.y. (h) 4 N HCl/EtOAc, r.t., 0.25–0.5 h, 58–96%.

because it is a solvatochromic probe whose absorbance and fluorescence spectra change depending on the polarity of the solvent environment. Also, a solution of **10** in ethanol has peak wavelengths that are measurable with a standard plate reader (λ_{Ex} = 430 nm/λ_{Em} = 480 nm).[18,19]

Compounds **6** and **7** were synthesized according to Scheme 1. According to the report by Gompel and Schuster,[20] **10** was prepared from **8** in a total yield of 25% (Scheme 1A). The common intermediate **15** was synthesized from **3** as a starting material (Scheme 1B). First, we tried to introduce fluorophore **10** into an ethyl ester aniline derivative, which was prepared by reduction of **12**. However, the fluorophore decomposed during basic hydrolysis of the ethyl ester. Therefore, fluorophore **10** was introduced after converting the ethyl ester motif of nitro derivative **12** into an MOM group. Then, MOM deprotection gave the target compound **7**. The synthesis of **6** was performed similarly.

Compounds **6** and **7** were evaluated in a reporter gene assay and a binding assay. We measured the transcriptional activity of human RXRα (hRXRα) induced by the RXR agonist NEt-TMN (**17**, Figure 2A) in the presence of **6** or **7**. The

https://dx.doi.org/10.1021/acs.jmedchem.0c01883
J. Med. Chem. 2021, 64, 861–870

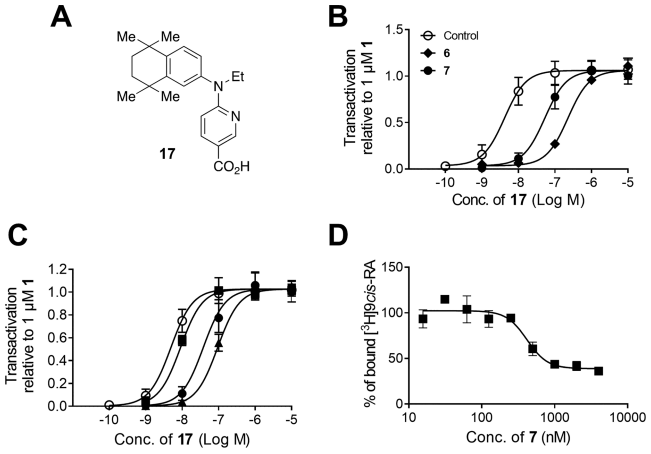

Figure 2. Transactivation of hRXRα by **17** in the absence or presence of **6** or **7**, and competitive binding assay using [^{3}H]9*cis*-RA. (A) The chemical structure of RXR agonist **17** (NEt-TMN). (B) Transactivation activity of **17** toward hRXRα in the absence or presence of **6** or **7**: **17** alone (open circles), 1 μM **6** (closed diamonds), or **7** (closed circles). Data are mean ± SD (n = 3). (C) Transactivation activity of **17** toward hRXRα in the absence or presence of **7**: **17** alone (open circles), 0.1 μM (closed squares), 1 μM (closed circles), and 3 μM (closed triangles) **7**. The data are shown as relative transactivation activity for the luciferase activity value of 1 μM **1**. Data are mean ± SD (n = 3). (D) Dose-dependent binding of [^{3}H]9*cis*-RA with hRXRα-LBD (50 nM) in the presence of **7**. The values are the percentage of bound [^{3}H]9*cis*-RA in the presence of **7**. Data are mean ± SD (n = 3).

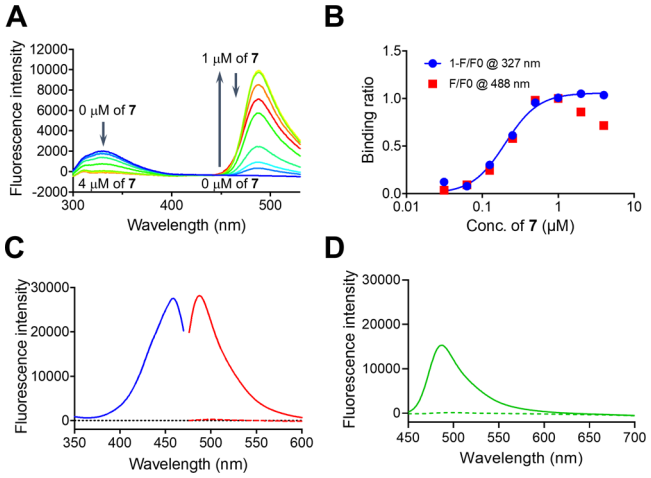

Figure 3. Changes in fluorescence intensity upon binding of **7** with hRXRα-LBD. (A) Fluorometric titration emission spectra of hRXRα-LBD (0.5 μM) upon addition of **7** (0–4 μM) in HEPES buffer (pH 7.9) at λ_{Ex} = 290 nm. (B) Binding ratio calculated as [1 − F_{327nm}/$F0_{327nm}$] (at 327 nm, blue) or [F_{488nm}/$F0_{488nm}$] (at 488 nm, red). $F0$ is the fluorescence intensity in the absence of **7** at each wavelength, and F is the observed fluorescence intensity. Curve fitting was performed using GraphPad Prism 8. (C) Fluorescence excitation and emission spectra of **7** (1 μM) in HEPES buffer in the absence (broken line) or presence (solid line) of hRXRα-LBD (0.5 μM). Excitation spectra and emission spectra were obtained at λ_{Em} = 487 nm and λ_{Ex} = 457 nm, respectively. (D) Emission spectra of **7** (1 μM) in HEPES buffer in the absence (broken line) or presence (solid line) of hRXRα-LBD at λ_{Ex} = 430 nm.

transcriptional-activity curve of **17** was shifted to the right by **6** or **7**, confirming that they are RXR antagonists (Figure 2B,C). The antagonist activity (pA_2) for hRXRα of **7** was 6.93, as determined by Schild analysis (Table 1). Moreover, **7** shows a

Table 1. Values of *Ki* and pA_2 for the hRXRα Receptor of NEt-3IB Related Compounds 5, 6, and 7

compound	*Ki*[a] (nM)	pA_2[c]
NEt-SB (**5**)	53[b]	8.2[d]
NEt-BA (**6**)	425	7.32
NEt-C343 (**7**)	332	6.93

[a]*Ki* values were calculated by a competitive binding assay using [^{3}H]9*cis*-RA. [b]Cited from ref 14. [c]pA_2 values were calculated from the transactivation activity toward hRXRα using Prism software. [d]Cited from ref 16.

preference for RXRα/γ over RXRβ (pA_2 = 5.76 for RXRβ, pA_2 = 6.49 for RXRγ) (Figure S1A,B), like **3**, which has the same main skeleton.[8] Interestingly, the slope of the Schild plot for **6** was 1.94, while that of **7** was 0.88 (Table S1). This result suggests that, whereas **7** is a competitive antagonist, **6** is not. The reason for this remains unclear at present. We next conducted a competitive binding test with **7** and [^{3}H]9*cis*-RA and observed dose-dependent replacement of [^{3}H]9*cis*-RA with **7** (Figure 2D). The *Ki* value of **7** was obtained to be 332 nM from the Cheng–Prusoff equation (Table 1).[21]

Once the antagonist activity and binding ability for hRXRα of **7** were confirmed, the fluorescence properties were investigated. The binding of **7** could be monitored by measuring the decreases in hRXRα-LBD fluorescence upon addition of increasing amounts of **7** (Figure 3A). The fluorescence around 330 nm due to Trp282 and Trp305 in hRXRα-LBD is quenched by ligand binding near these residues.[22,23] As expected, the fluorescence at the maximum fluorescence wavelength of around 330 nm (327 nm) was quenched by **7** in a dose-dependent manner. The binding ratio at 327 nm was calculated based on the reported method (see the Experimental Section), and the dissociation constant (*Kd*) for hRXRα-LBD of **7** was determined to be 200 nM from the binding ratio at 327 nm (Figure 3B).[23] Interestingly, an increase in the fluorescence intensity derived from **7** was observed at 488 nm (Figure 3A right). The *Kd* at the maximum fluorescence wavelength of 488 nm at a concentration of 1 μM or less was correlated with that at 327 nm. On the other hand, precipitation of **7** occurred at more than 2 μM (Figure 3B). Based on this result, we decided to investigate the fluorescence properties further.

First, the fluorescence characteristics of **7** were examined with a fluorescence spectrophotometer. The maximum absorbance wavelength of **7** in the presence of hRXRα-LBD was 457 nm, and the maximum fluorescence wavelength was 487 nm (Figure 3C). The fluorescence intensity of **7** in the absence of hRXRα-LBD was extremely low, judging from the fluorescence spectrum and fluorescence quantum yield (Figure 3C, Table 2, Figure S2). This suggests that **7** emits fluorescence at 487 nm only when it is bound to hRXRα-LBD. Next, an excitation filter of 430 nm was selected for a standard fluorescence plate reader as being in the vicinity of the maximum excitation wavelength; the fluorescence spectrum at this excitation wavelength had a maximum emission wavelength of 487 nm (Figure 3D). Based on this result, we assumed that λ_{Em} = 535 nm, used for FITC, would provide a sufficient fluorescence intensity. The fluorescence intensity of

https://dx.doi.org/10.1021/acs.jmedchem.0c01883
J. Med. Chem. 2021, 64, 861–870

Table 2. Absorbance and Fluorescence Properties of 7

compound	condition	λ_{Abs}	ε (cm^{-1}/M)	λ_{Em}	Φ[a]
fluorescein	1 mM NaOH/EtOH	500	9.23×10^4	522	0.92[b]
	0.1 M NaOHaq	490	9.23×10^4	512	0.93[c]
7	1% DMSO in EtOH	450	5.36×10^4	490	0.0549 ± 0.0005[d]
	1% DMSO in HEPES buffer (pH 7.9)	450	2.95×10^4	497	0.0118 ± 0.0022[d]
	1% DMSO in HEPES buffer (pH 7.9) (with RXRα-LBD)	460	4.07×10^4	487	0.596 ± 0.023[d]

[a]Fluorescence quantum yield was determined by integrating the digitized emission spectra from 455 to 650 nm at 450 nm excitation on a Shimadzu spectrofluorophotometer RF-6000, referencing the integral to that for 100 nM fluorescein in 1 mM NaOH/EtOH or 0.1 M NaOHaq. Calculations were done with LabSolutions. The indexes of refraction for the solvents are 1.361 and 1.333 for ethanol and water, respectively. [b]Cited from ref 24. [c]Cited from ref 25. [d]Data are mean ± SD (n = 3).

7 at λ_{Ex} = 430 nm/λ_{Em} = 535 nm increased with a decrease of the solvent polarity (Figure S3).

Coumarin 343 (**10**), which was introduced as a fluorescent moiety, is known to show a pH-dependent change of the maximum absorption wavelength in aqueous solution.[26,27] When the carboxyl group of **10** is ionized in aqueous solution, the conjugated structure of **10** is stabilized, and a fluorescence peak appears at around 456 nm. On the other hand, this does not occur with **7** because the carboxyl is in amide form. This is the reason why **7** does not show solvatochromism like that of **10**. We consider that, in water and HEPES buffer (pH 7.9), the carboxyl group of the nicotinic acid moiety of **7** was ionized and nitrogen in julolidine is protonated, reducing its electron-donating character, as in conformation I (Figure 4A). On the other hand, in a low-polarity environment, the carboxyl group in the nicotinic acid moiety would not be ionized, so the fluorescence intensity would increase due to the electron-donating character of the nitrogen in julolidine (Figure 4A). It has been reported that conversion of the carboxy group of **10** to amide increases the fluorescence intensity in 1,4-dioxane, which is a nonpolar solvent.[28] Such a solvent polarity-dependent fluorescence intensity change reflects the degree of intramolecular charge transfer (ICT) in the excited state.[29−31]

Compound **7** is considered to emit strong fluorescence in a low-polarity environment because it takes the resonance structure II in the excited state (Figure 4A). Based on the strong fluorescence emission upon binding of **7** with RXRα, we inferred that the fluorophore moiety occupies the RXR binding pocket. The binding structure of **7** in the antagonistic form in the RXR-ligand binding pocket (LBP) was examined. We have already reported docking simulations on AutoDock[32] using an X-ray structure of the RXR antagonistic form (PDB: 3A9E[33]), which predicted that **5** would have a similar binding mode to RXR antagonist LG100754 (**18**) in the RXR-LBD.[16] This time, docking simulation using AutoDock vina[34] was performed. As a result, all compounds gave similar binding modes in the most stable complexes to that of **18**, which forms a hydrogen bond with the carboxy group with Arg 321 in the RXR-LBD (Figure 4B,C). In the case of **6**, the benzanilide moiety can exist inside (mode 1) or outside (mode 2) the RXR-LBD, and the difference of binding affinity energy is only 0.1 kcal/mol. Interestingly, surveying the docking profiles of **7** provided another structure (mode 6, yellow) in which the carboxylic acid moiety of **7** is not located close to Arg321 and in which the coumarin-343 fluorophore exists inside the LBP (Figure 4C, Movie S1). This structure, in which the fluorophore is located in a hydrophobic region inside RXR-LBD, is consistent with the results of the fluorescence experiments, though the binding affinity energy of mode 6 was higher than that of mode

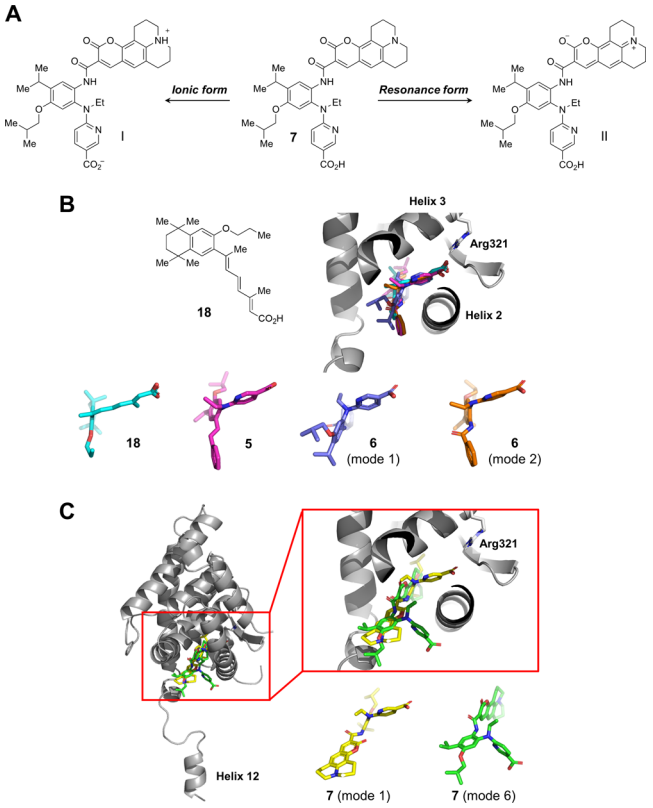

Figure 4. Putative structures of **7** that bind to RXRα-LBD and emit fluorescence. (A) Ionic and resonance structures of **7**. The ionic form I is favored in water, while the resonance form II is considered to be the fluorescent form. (B) Chemical structure of LG10075416 (**18**), binding structure of **18** (cyan), and the most stable binding structures of **5** (magenta), **6** (mode 1, purple), and **6** (mode 2, orange) in the antagonistic form with RXRα-LBD (PDB code: 3A9E)[33] predicted by AutoDock vina.[34] (C) Putative models of **7** with RXRα-LBD (PDB code: 3A9E) generated by AutoDock vina.

1 by 1.9 kcal/mol. Recently, we succeeded in obtaining an X-ray crystal structure of the RXR antagonist CBTF-EE (**19** Figure S4) with the RXRα-LBD (PDB: 7CFO).[35] The data show that **19** binds to the entrance of the LBP, and the carboxylic acid moiety of **19** is located outside the LBP, while the ethoxy ethyl group invades the internal region of the LBP. These findings support binding mode 6. However, a cocrystal structure analysis will be needed to enable detailed discussion.

Next, we attempted to construct a new fluorescence binding assay by utilizing the fluorescence intensity change upon binding of **7** with hRXRα-LBD. Indeed, the dose-dependent binding of hRXRα-LBD to 0.1 μM **7** was confirmed (Figure 5A) by using the procedure illustrated in Figure S5 on a 384-

https://dx.doi.org/10.1021/acs.jmedchem.0c01883
J. Med. Chem. 2021, 64, 861−870

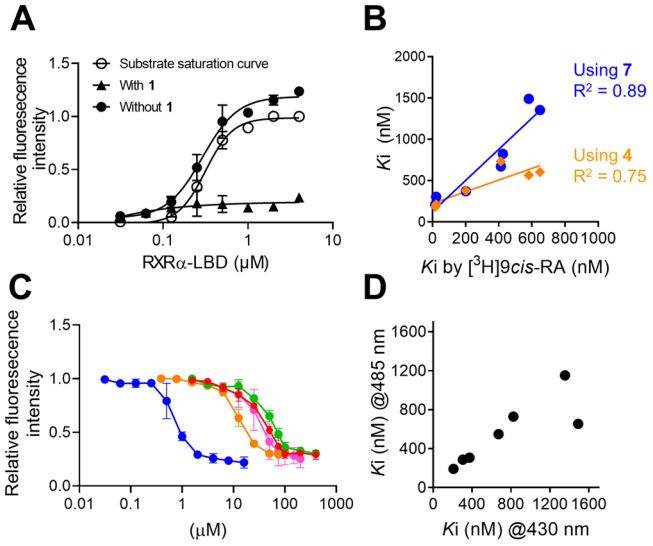

Figure 5. Fluorescence binding assay data using **7** at λ_{Ex} = 430 nm/ λ_{Em} = 535 nm. (A) Substrate saturation curve depending on the concentration of hRXRα-LBD in the presence of 0.1 μM **7**. The substrate saturation curve was calculated by subtracting "with 10 μM **1** (circles)" from "without **1** (triangles)". Data are mean ± SD (n = 3). (B) Correlation of binding affinity values toward hRXRα-LBD obtained with **7** (blue) or **4** (orange) to those obtained with [^{3}H]9*cis*-RA. (C) Relative fluorescence intensity curves of natural ligands using **7**, 9*cis*-RA (blue), DHA (red), EPA (green), arachidonic acid (orange), and honokiol (pink). Data shown are mean ± SD (n = 3). (D) Correlation of *Ki* values toward hRXRα-LBD obtained by using **7** at λ_{Ex} = 430 nm and 485 nm.

well plate. Besides, the fluorescence intensity in the presence of 10 μM **1** was clearly decreased. Analysis of the substrate saturation curve gave a Hill coefficient of 2.78 for **7**, and *Kd* was 257 nM, which is very close to the value obtained from the fluorescence quenching experiment with hRXRα-LBD (*Kd* = 200 nM). Moreover, **7** showed positive cooperativity because the Hill coefficient was more than 1, suggesting that once **7** binds to hRXRα-LBD, it promotes the binding of additional **7**. We also examined the time-dependent change of the *Z′* factor as a measure of the quality of the screening, and it was 0.5 or more at λ_{Ex} at all time points, indicating that this assay is stable (Figure S6).

The *Ki* values of well-known rexinoids (Figure S7) were next measured using 100 nM **7** and 500 nM hRXRα-LBD, and the results were compared with the reported *Ki* values using **4** or [^{3}H]9*cis*-RA. The specific binding of each compound is shown in Figure S8A. The IC_{50} value was calculated from each curve, and *Ki* was calculated using the Cheng−Prusoff equation (Table S2). When we compared the *Ki* values with those obtained using [^{3}H]9*cis*-RA, **7** showed a higher correlation (R^2 = 0.89) than did **4** (R^2 = 0.75) (Figure 5B). The differences of individual *Ki* values between **7** and [^{3}H]9*cis*-RA are likely to be due to factors such as differences in the source of the hRXRα-LBD or in the assay temperature. In particular, TBTCl and NEt-4IB, which have weak binding properties, showed poor agreement between the *Ki* values obtained using RI and **4**. However, the binding assay with **7** showed better agreement with the RI values (Table S2). Based on these results, we consider that the assay using **7** is suitable for use as a replacement for the general binding assay using [^{3}H]9*cis*-RA. Because polyunsaturated fatty acids (such as EPA, DHA, and arachidonic acid), 9*cis*-RA, and honokiol are natural ligands, their binding ability to RXR was also examined (Figure 5C). The *Ki* value of 9*cis*-RA was determined to be 478 nM, which is higher than the *Ki* value obtained using [^{3}H]9*cis*-RA, as was the case with the other known compounds. Polyunsaturated fatty acids and honokiol, which have a weak binding affinity (ca. 30−100 μM),[36] also caused fluorescence intensity changes. We examined if FITC filters (λ_{Ex} = 485 nm/ λ_{Em} = 535 nm) would work for this assay (Figure 5D). The *Z′* factor at the excitation wavelength of 485 nm was almost the same as that at 430 nm, suggesting that the 485 nm filter set can also be used as an alternative to the 430 nm filter (Figure S6). The *Ki* values obtained at excitation wavelengths of 430 and 485 nm were almost identical, except for NEt-4IB (Figure 5D). However, NEt-4IB is known to be a partial agonist, and the decrease in the maximum efficacy would strongly influence the IC_{50} value used for calculating the *Ki* value (Figure S8D). Since the absorbance at 485 nm is lower than that at 430 nm and there is an overlap between the absorbance and the fluorescence wavelengths (Figure S2 and Figure 3C), the sensitivity at 430 nm is higher than that at 485 nm.

CONCLUSIONS

The developed binding assay using fluorescent RXR antagonist **7** is rapid, simple, and nonhazardous and can be run with a standard plate reader. Further, since **7** emits strong fluorescence only when bound to hRXRα-LBD, the assay does not require B/F separation. The *Ki* values of various compounds in this assay were well correlated with the corresponding *Ki* values obtained using [^{3}H]9*cis*-RA. This method appears to be suitable to replacing the current binding assay using [^{3}H]9*cis*-RA, and we think that it will prove useful not only for drug discovery but also for research on endocrine disruptors, functional foods, and natural products.

EXPERIMENTAL SECTION

Chemistry. *General.* All solvents and chemicals were used as purchased without further purification. The progress of all reactions was monitored by thin layer chromatography (TLC) on 0.2 mm-thick TLC plates (Merck, glass-backed, silica gel 60 F245), and spots were detected under UV light. Purification was done by flash column chromatography on silica gel 60 (Kanto Chemical, particle size 0.04−0.05 mm). ^{1}H NMR and ^{13}C NMR spectra were measured on a Varian Mercury-300 (^{1}H 300 MHz, ^{13}C 75 MHz) spectrometer or a Varian 400-MR (^{1}H 400 MHz, ^{13}C 100 MHz) spectrometer at room temperature. Deuterated chloroform and dimethyl sulfoxide ($CDCl_3$ and DMSO-d_6) were used as solvents in all routine NMR measurements. Chemical shifts are reported in ppm relative to the respective deuterated solvent peak, $CHCl_3$ (δ 7.26 ppm), DMSO-d_6 (δ 2.50 ppm) for ^{1}H NMR and $CDCl_3$ (δ 77 ppm) for ^{13}C NMR, and coupling constants are given in Hz. FAB-MS spectra were measured on a JEOL JMS-700 mass spectrometer. Electrospray ionization (ESI) mass spectra were measured on a Bruker HCT (LRMS) or MicrOTOF (HRMS). Melting points were determined with a J-Science RFS-10 hot stage microscope. Elemental analysis was carried out with a PerkinElmer 2400 Series II CHNS/O elemental analyzer, and results were within ±0.4% of the theoretical values. The purity of all tested compounds was >95%, as confirmed by HPLC.

Analytical HPLC. Analytical HPLC was performed using a Shimadzu liquid chromatographic system (Kyoto, Japan) consisting of an LC-20AT pump, SPD-20A UV−vis spectrophotometric detector, CTO-10ASvp column oven, and LabSolutions software. Samples (each 20 μL) were injected onto an Inertsil ODS-3 column (4.6 i.d. × 100 mm, 3 μm, GL Sciences, Tokyo, Japan) fitted with a guard column of Inertsil ODS-3 (4.0 mm i.d. × 10 mm, 3 μm, GL Sciences) at 40 °C, using MeOH/H_2O (95:5 or 80:20 + 0.1% formic

https://dx.doi.org/10.1021/acs.jmedchem.0c01883
J. Med. Chem. 2021, 64, 861−870

acid, v/v) as the mobile phase. The flow rate was 0.7 mL/min, and the absorbance at 260 nm was monitored.

*6-[N-Ethyl-N-(2-benzamido-5-isobutoxy-4-isopropylphenyl)-amino]nicotinic Acid (**6**).* **16a** (92 mg, 0.18 mmol) was dissolved in 4 N HCl/EtOAc (1 mL). The solution was stirred at room temperature for 0.25 h, then evaporated under reduced pressure, and neutralized with sat. $NaHCO_3$ aq. The aqueous layer was extracted with EtOAc (3 × 20 mL). The combined organic layer was washed with H_2O (2 × 20 mL) and brine (20 mL) and then dried over $MgSO_4$. The solvent was evaporated under reduced pressure to afford 82 mg of **6** as a white solid (96%), which was recrystallized from EtOAc/*n*-hexane to afford 60 mg of **6** as white needles. mp 193.1−194.5 °C. ^{1}H-NMR (400 MHz, $CDCl_3$): δ 8.96 (1H, dd, J = 2.4, 1.0 Hz), 8.37 (1H, brs), 7.94 (1H, dd, J = 8.8, 2.4 Hz), 7.85 (1H, br s), 7.59−7.57 (2H, m), 7.48 (1H, tt, J = 7.3, 1.5 Hz), 7.41−7.36 (2H, m) or 7.38 (2H, tt, J = 7.3, 1.5 Hz), 6.63 (1H, s), 6.25 (1H, dd, J = 8.8, 1.0 Hz), 4.05 (2H, s), 3.67 (2H, d, J = 6.6 Hz), 3.40 (1H, sep, J = 6.8 Hz), 2.13 (1H, sep, J = 6.6 Hz), 1.32 (6H, d, J = 6.8 Hz), 1.28 (3H, t, J = 6.8 Hz), 1.06 (6H, d, J = 6.6 Hz). ^{13}C-NMR (100 MHz, $CDCl_3$): δ: 171.23, 170.78, 165.20, 160.54, 154.09, 151.98, 138.97, 134.53, 131.79, 128.80, 128.29, 126.67, 120.77, 115.08, 110.68, 107.32, 74.62, 60.40, 45.13, 28.45, 27.28, 22.46, 21.01, 19.36, 14.15, 13.06. Calcd for $C_{28}H_{33}N_3O_4$: C, 70.71; H, 6.99; N, 8.84. Found: C, 70.45; H, 7.08; N, 8.71. HRMS (ESI$^-$) m/z: [M − H]$^-$ Calcd for $C_{28}H_{32}N_3O_4$ 474.2398; Found 474.2402. Analytical HPLC (MeOH/H_2O = 80:20 + 0.1% formic acid): 8.7 min; 99.80% purity.

*6-[N-Ethyl-N-(5-isobutoxy-4-isopropyl-2-(11-oxo-2,3,6,7-tetrahydro-1H,5H,11H-pyrano[2,3-f]pyrido[3,2,1-ij]quinoline-10-carboxamido)phenyl)amino]nicotinic Acid (**7**).* A solution of **16b** (105 mg, 0.15 mmol) in 4 N HCl/EtOAc (4 mL) was stirred at room temperature for 0.5 h and then evaporated under reduced pressure. The residue was recrystallized from EtOH/EtOAc to afford 65 mg of **7** as an orange solid (58%). mp 293.8−296.1 °C. ^{1}H-NMR (400 MHz, $CDCl_3$): δ 10.99 (1H, s), 9.03 (1H, s), 8.59 (1H, s), 8.38 (1H, s), 8.18 (1H, d, J = 7.4 Hz), 6.99 (1H, s), 6.60 (1H, s), 6.50 (1H d, J = 7.4 Hz), 4.34 (2H, q, J = 7.1 Hz), 3.68 (2H, d, J = 6.0 Hz), 3.40 (1H, sep, J = 3.0 Hz), 3.35 (2H, t, J = 5.8 Hz), 3.33 (2H, t, J = 6.8 Hz), 2.85 (2H, t, J = 6.2 Hz), 2.77 (2H, t, J = 6.0 Hz), 2.14 (1H, sep, J = 6.5 Hz), 1.96 (4H, m), 1.42 (3H, t, J = 7.1 Hz), 1.33−1.28 (8H, m), 1.07 (6H, d, J = 6.5 Hz). ^{13}C-NMR (75 MHz, $CDCl_3$): δ 175.61, 171.14, 163.95, 163.40, 161.82, 153.99, 152.92, 152.43, 148.78, 148.12, 140.94, 139.67, 127.69, 127.28, 127.08, 121.37, 120.07, 116.85, 108.15, 106.66, 105.45, 74.53, 60.21, 50.08, 49.66, 48.35, 28.14, 27.14, 27.06, 22.13, 22.04, 20.79, 20.70, 19.63, 19.08, 13.90, 12.18. Calcd for $C_{37}H_{42}N_4O_6 \cdot 1/2\ H_2O$: C, 68.61; H, 6.69; N, 8.65. Found: C, 68.41; H, 6.58; N, 8.57. HRMS (ESI$^-$) m/z: [M − H]$^-$ Calcd for $C_{37}H_{41}N_4O_6$ 637.3032; Found 637.3035. Analytical HPLC (MeOH/H_2O = 95:5 + 0.1% formic acid): 6.3 min; 95.03% purity.

*Ethyl 11-Oxo-2,3,6,7-tetrahydro-1H,5H,11H-pyrano[2,3-f]-pyrido[3,2,1-ij]quinoline-10-carboxylate (**9**).* 2,3,6,7-Tetrahydro-8-hydroxy-1*H*,5*H*-benzo[*ij*]quinolizine-9-carboxaldehyde (435 mg, 2.0 mmol) was added to a mixture of diethyl malonate (**8**) (1.0 mL, 66 mmol) and piperidine (390 μL, 4.0 mmol). The reaction mixture was stirred at 30 °C for 3 h, and then H_2O (10 mL) was added to afford a brown precipitate, which was collected and dissolved in EtOAc (120 mL). The solution was washed with H_2O (2 × 120 mL) and brine (120 mL), dried over $MgSO_4$, filtered, and evaporated under reduced pressure. The residue was purified by flash column chromatography (*n*-hexane/EtOAc = 2:1) to afford 272 mg of **9** as colorless needles (43%). ^{1}H-NMR (300 MHz, $CDCl_3$): δ 8.32 (1H, s), 6.04 (1H, s), 4.36 (2H, q, J = 7.2 Hz), 3.34 (2H, t, J = 5.6 Hz), 3.32 (2H, t, J = 5.6 Hz), 2.88 (2H, t, J = 6.5 Hz), 2.76 (2H, t, J = 6.0 Hz), 2.01−1.92 (4H, m), 1.38 (3H, t, J = 7.2 Hz).

*11-Oxo-2,3,6,7-tetrahydro-1H,5H,11H-pyrano[2,3-f]pyrido-[3,2,1-ij]quinoline-10-carboxylic Acid (Coumarin 343, **10**).* A solution of **9** (238 mg, 0.76 mmol) in conc. HCl (7.0 mL) was stirred at room temperature for 20 h and then cooled to 0 °C, and 28% NH_3aq was added to it. The resulting orange precipitate was collected and recrystallized from DMSO/CH_3CN to afford 128 mg of **10** as orange needles (59%). ^{1}H-NMR (400 MHz, DMSO-d_6): δ 11.59 (1H, s), 7.60 (1H, s), 6.39 (1H, s), 1.87 (2H, t, J = 6.5 Hz), 1.85 (2H, t, J = 6.5 Hz), 1.66 (2H, t, J = 1.9 Hz), 1.65 (2H, t, J = 1.9 Hz), 1.02 (4H, m). MS (ESI$^-$) m/z: 284 [M − H] $^-$.

*Ethyl 6-[N-Ethyl-N-(5-isobutoxy-4-isopropylphenyl)amino]-nicotinate (**11**).* To a solution of **3** (356 mg, 1.0 mmol) in EtOH (10 mL) was added concentrated H_2SO_4 (160 μL, 3.0 mmol). The reaction mixture was refluxed for 21 h and then poured into ice water (50 mL). The aqueous layer was extracted with EtOAc (2 × 100 mL). The combined organic layer was washed with H_2O (2 × 100 mL) and brine (50 mL) and dried over $MgSO_4$. The solvent was evaporated under reduced pressure to afford 385 mg of **11** as a brown oil (q.y.). ^{1}H-NMR (300 MHz, $CDCl_3$): δ 8.86 (1H, d, J = 2.3 Hz), 7.80 (1H, dd, J = 9.1, 2.3 Hz), 7.25 (1H, d, J = 8.1 Hz), 6.76 (1H, dd, J = 8.1, 2.0 Hz), 6.64 (1H, d, J = 2.0), 6.25 (1H, d, J = 9.1 Hz), 4.32 (2H, q, J = 7.2 Hz), 4.03 (2H, q, J = 6.8 Hz), 3.67 (2H, d, J = 6.0 Hz), 3.36 (1H, sep, J = 6.9 Hz), 2.12 (1H, sep, J = 6.8 Hz), 1.35 (3H, t, 7.2 Hz), 1.26 (6H, d, J = 6.9 Hz), 1.24 (3H, t, J = 6.8 Hz), 1.06 (6H, d, J = 6.8 Hz).

*Ethyl 6-[N-Ethyl-N-(5-isobutoxy-4-isopropyl-2-nitrophenyl)-amino]nicotinate (**12**).* To a solution of **11** (910 mg, 2.4 mmol) in Ac_2O (12 mL) was added a mixture of concentrated HNO_3 (0.5 mL, 7.2 mmol) and Ac_2O (1.6 mL) on ice. The reaction mixture was stirred at room temperature for 0.5 h and then neutralized with sat. $NaHCO_3$ aq. The aqueous layer was extracted with EtOAc (3 × 50 mL). The combined organic layer was washed with H_2O (2 × 100 mL) and brine (100 mL) and dried over $MgSO_4$. The solvent was evaporated under reduced pressure, and the residue was purified by flash column chromatography (*n*-hexane/EtOAc = 10:1) to afford 768 mg of **12** as a brown oil (75%). ^{1}H-NMR (300 MHz, $CDCl_3$): δ 8.82 (1H, d, J = 2.4 Hz), 8.02 (1H, s), 7.93 (1H, dd, J = 9.0, 2.4 Hz), 6.69 (1H, s), 6.24 (1H, d, J = 9.0 Hz), 4.32 (2H, q, 7.2 Hz), 3.78 (2H, d, J = 6.4 Hz), 3.36 (1H, sep, J = 6.9 Hz), 2.16 (1H, sep, J = 6.4 Hz), 1.35 (3H, t, J = 7.2 Hz), 1.32−1.24 (11H, m), 1.07 (6H, d, J = 6.4 Hz). ^{13}C-NMR (75 MHz, $CDCl_3$): δ 165.86, 161.05, 159.68, 150.96, 139.52, 138.13, 137.41, 137.21, 124.35, 115.83, 112.94, 106.30, 75.05, 60.35, 45.83, 28.27, 27.00, 22.05, 20.99, 19.18, 14.30, 13.08.

*6-[N-Ethyl-N-(5-isobutoxy-4-isopropyl-2-nitrophenyl)amino]-nicotinic Acid (**13**).* To a solution of **12** (669 mg, 1.56 mmol) in EtOH (8 mL) was added 2 N NaOHaq (8 mL). The mixture was stirred at 80 °C for 1 h and then evaporated under reduced pressure. The residue was poured into 2 N HCl aq. and extracted with EtOAc (50 mL × 2). The combined organic layer was washed with H_2O (2 × 50 mL) and brine (50 mL) and dried over $MgSO_4$. The solvent was evaporated under reduced pressure to afford 530 mg of **13** as a yellow solid (85%). ^{1}H-NMR (400 MHz, $CDCl_3$): δ 8.88 (1H, d, J = 2.2 Hz), 8.03 (1H, s), 7.96 (1H, dd, J = 9.1, 2.2 Hz), 6.68 (1H, s), 6.23 (1H, d, J = 9.1 Hz), 3.78 (2H, d, J = 6.3 Hz), 3.36 (1H, sep, J = 6.9 Hz), 2.17 (1H, sep, J = 6.6 Hz), 1.32−1.26 (11H, m), 1.07 (6H, d, J = 6.6 Hz). ^{13}C-NMR (100 MHz, $CDCl_3$): δ 171.35, 161.15, 160.14, 151.90, 139.37, 138.62, 137.70, 136.92, 124.43, 114.67, 113.02, 106.53, 75.10, 45.95, 28.26, 27.02, 22.04, 19.19, 13.02. MS (ESI$^-$) m/z: 400 [M − H] $^-$.

*Methoxymethyl 6-[N-Ethyl-N-(5-isobutoxy-4-isopropyl-2-nitrophenyl)amino]nicotinate (**14**).* To a solution of **13** (476 mg, 1.20 mmol) in anhydrous DMF (8 mL) were added chloromethyl methyl ether (0.1 mL, 1.3 mmol) and triethylamine (0.18 mL, 1.3 mmol) under an Ar atmosphere. The mixture was stirred on ice for 1 h and then neutralized with sat. NH_4Claq. The aqueous layer was extracted with EtOAc (3 × 50 mL). The combined organic layer was washed with H_2O (2 × 50 mL) and brine (50 mL) and dried over $MgSO_4$. The solvent was evaporated under reduced pressure to afford 629 mg of **14** as a yellow oil (q.y.). ^{1}H-NMR (400 MHz, $CDCl_3$): δ 8.86 (1H, d, J = 2.1 Hz), 8.03 (1H, s), 7.96 (1H, dd, J = 8.5, 2.1 Hz), 6.71 (1H, s), 6.26 (1H, d, J = 8.5 Hz), 5.43 (2H, s), 3.80 (2H, d, J = 6.0 Hz), 3.51 (3H, s), 3.38 (1H, sep, J = 6.9 Hz), 2.17 (1H, sep, J = 6.7 Hz), 1.32−1.24 (11H, m), 1.08 (6H, d, J = 6.7 Hz). ^{13}C-NMR (100 MHz, $CDCl_3$): δ 165.29, 161.13, 159.95, 151.35, 139.46, 138.33, 137.58, 137.05, 124.39, 115.09, 112.95, 106.46, 90.28, 75.10, 57.51, 45.92, 28.28, 27.03, 22.06, 19.21, 14.15, 13.08. MS (FAB$^+$) m/z: 446 [M + H]$^+$.

https://dx.doi.org/10.1021/acs.jmedchem.0c01883
J. Med. Chem. 2021, 64, 861−870

*Methoxymethyl 6-[N-Ethyl-N-(2-amino-5-isobutoxy-4-isopropylphenyl)amino]nicotinate (**15**).* To a solution of **14** (100 mg, 0.22 mmol) in EtOH (5 mL) was added 10% activated Pd-C (catalytic amount). The reaction mixture was stirred under a H_2 atmosphere at room temperature for 3 h and filtered through Celite, which was then washed with EtOAc. The filtrate was evaporated under reduced pressure to afford 81.2 mg of **15** as a brown oil (81%). ^{1}H-NMR (400 MHz, $CDCl_3$): δ 8.91 (1H, d, J = 2.4 Hz), 7.88 (1H, dd, J = 9.0, 2.4 Hz), 6.74 (1H, s), 6.50 (1H, s), 6.17 (1H, d, J = 9.0 Hz), 5.44 (2H, s), 4.12 (1H, sext, J = 6.9 Hz), 3.87 (1H, sext, J = 6.9 Hz), 3.60 (2H, d, J = 6.6 Hz), 3.52 (3H, s), 3.32 (1H, sep, J = 6.6 Hz), 2.10 (1H, sep, J = 6.5 Hz), 1.29−1.22 (11H, m), 1.03 (6H, d, J = 6.5 Hz). ^{13}C-NMR (100 MHz, $CDCl_3$): δ 165.49, 160.33, 151.52, 149.91, 138.30, 136.58, 125.71, 114.97, 114.15, 112.02, 107.11, 90.15, 74.94, 57.46, 43.91, 28.50, 26.82, 22.64, 22.53, 19.37, 13.09. MS (FAB$^+$) m/z: 416 [M + H]$^+$.

*Methoxymethyl 6-[N-Ethyl-N-(2-benzamido-5-isobutoxy-4-isopropylphenyl)amino]nicotinate (**16a**).* To a solution of **15** (83.0 mg, 0.2 mmol) in anhydrous CH_2Cl_2 (2 mL) were added benzoyl chloride (29 mL, 0.25 mmol) and *N*,*N*-diisopropylethylamine (68 mL, 0.4 mmol) under an Ar atmosphere. The mixture was stirred at room temperature for 17 h and then poured into ice water (20 mL). The aqueous layer was extracted with EtOAc (2 × 40 mL). The combined organic layer was washed with H_2O (2 × 40 mL) and brine (40 mL) and dried over $MgSO_4$. The solution was evaporated under reduced pressure, and the residue was purified by flash column chromatography (*n*-hexane/EtOAc = 4:1) to afford 95 mg of **16a** (90%). ^{1}H-NMR (400 MHz, $CDCl_3$) δ: 8.96 (1H, dd, J = 2.4, 0.8 Hz), 8.39 (1H, s), 7.94 (1H, dd, J = 8.8, 2.4 Hz), 7.90 (1H, br s), 7.61−7.58 (2H, m), 7.49−7.45 (1H, m), 7.40−7.36 (2H, m), 6.65 (1H, s), 6.25 (1H, dd, J = 9.0, 0.6 Hz), 5.44 (2H, s), 4.06 (2H, d, J = 6.4 Hz), 3.68 (2H, d, J = 6.5 Hz), 3.51 (3H, s), 3.41 (1H, sep, J = 7.0 Hz), 2.13 (1H, sep, J = 6.5 Hz), 1.33 (6H, d, J = 7.0 Hz), 1.29 (3H, t, J = 6.4 Hz), 1.06 (6H, d, J = 6.5 Hz). ^{13}C-NMR (100 MHz, $CDCl_3$) δ: 165.21, 165.01, 160.43, 154.01, 151.51, 138.60, 137.90, 134.63, 131.73, 131.05, 128.78, 128.46, 126.63, 120.55, 115.39, 110.73, 107.26, 90.40, 74.65, 57.56, 45.02, 28.45, 27.31, 22.48, 19.35, 13.11. MS (FAB$^+$) m/z: 520 [M + H]$^+$.

*Methoxymethyl 6-[N-Ethyl-N-(5-isobutoxy-4-isopropyl-2-(11-oxo-2,3,6,7-tetrahydro-1H,5H,11H-pyrano[2,3-f]pyrido[3,2,1-ij]-quinoline-10-carboxamido)phenyl)amino]nicotinate (**16b**).* To a solution of **15** (57.0 mg, 0.2 mmol) and **10** (83.1 mg, 0.2 mmol) in anhydrous DMF (5 mL) were added EDCI·HCl (46 mg, 0.24 mmol) and HOBt (32.4 mg, 0.24 mmol) under an Ar atmosphere. The mixture was stirred at room temperature for 10 h and then poured into H_2O (40 mL). The aqueous layer was extracted with EtOAc (3 × 40 mL). The combined organic layer was washed with H_2O (2 × 40 mL) and brine (40 mL) and dried over $MgSO_4$. The solution was evaporated under reduced pressure, and the residue was purified by flash column chromatography (*n*-hexane/EtOAc = 2:1) to afford 136 mg of **16b** (q.y.). ^{1}H-NMR (300 MHz, $CDCl_3$): δ 10.99 (1H, s), 8.93 (1H, d, J = 2.2 Hz), 8.58 (1H, s), 8.54 (1H, s), 7.81 (1H, dd, J = 9.1, 2.2 Hz), 6.90 (1H, s), 6.58 (1H,s), 6.12 (1H, d, J = 9.1 Hz), 5.38 (2H, d, J = 2.2 Hz), 4.31 (1H, sext, J = 6.8 Hz), 3.84 (1H, sext, J = 6.8 Hz), 3.63 (2H, d, J = 6.6 Hz), 3.47 (3H, s), 3.37 (1H, sep, J = 7.0 Hz), 3.24 (4H, s), 2.76 (2H, t, J = 6.2 Hz), 2.69 (2H, t, J = 6.2 Hz), 2.08 (1H, sep, J = 6.6 Hz), 1.88 (4H, s), 1.31−1.23 (9H, m), 1.02 (6H, d, J = 6.6 Hz). ^{13}C-NMR (75 MHz, $CDCl_3$): δ 165.43, 162.76, 161.24, 160.55, 153.18, 152.46, 151.53, 148.19, 147.67, 137.87, 137.35, 130.34, 129.56, 126.86, 119.87, 119.58, 114.33, 111.30, 108.50, 108.14, 106.93, 105.42, 90.00, 74.45, 57.36, 50.05, 49.62, 44.28, 28.34, 27.23, 27.09, 22.38, 20.89, 20.85, 19.88, 19.26, 14.04, 12.70. MS (FAB$^+$) m/z: 683 [M + H]$^+$.

Docking Simulation. The crystal structure of the human RXRα-LBD was retrieved from the Brookhaven Protein Data Bank: http://www.rcsb.org/pdb/Welcome.do. (3A9E).[33] Polar hydrogen atoms were added using AutoDockTools (ADT).[32] United atom Kollman charges were assigned for the protein. The 3D structures of ligands used for the docking study were constructed using ChemDraw and Chem3D. These ligands were energetically minimized by using Molecular Mechanics (MM) and semiempirical molecular orbital calculation (MOPAC, PM3).[37] The AutoDock vina molecular docking program[34] was employed, using a genetic algorithm with local search (GALS). One hundred individual GA runs, 100 chromosomes, a crossover ratio of 0.80, a rate of gene mutation of 0.02, and an elitism ratio of 0.10 were used for each ligand. PyMOL 2.4 was used for molecular modeling.

In Vitro Assays. *Reporter Gene Assay.* Luciferase reporter gene assays using COS-1 cells were performed as reported previously.[9,38]

Ligand Binding Assay and Kd Determination Using [^{3}H]9cis-RA. The competitive binding assay using 9-*cis*-[11,12-^{3}H]-retinoic acid ([^{3}H]9*cis*-RA) was performed as described.[9,39,40]

UV−vis and Fluorescence Spectra Measurements. Absorbance spectra were recorded on a Jasco UV−vis spectrophotometer model V-530. Fluorescence spectra were recorded on a Shimadzu spectrofluorometer model RF-6000. The sample quartz cuvette path length was 1 cm or 5 mm, and the excitation and emission slit widths were set at 5 nm. Analytical-grade solvents were obtained from Wako and used as received. The relative fluorescence intensity of 1 μM **7** in various solvents containing 1% DMSO was determined at λ_{Ex} = 430 nm/λ_{Em} = 535 nm.

Determination of Fluorescence Quantum Yield. The fluorescence quantum yield of **7** was determined as described elsewhere.[24] Briefly, the excitation wavelength was chosen based on the UV−vis absorbance spectrum of 10 μM **7** and fluorescein in 1 mM NaOH/EtOH (see Figure S2). Then the excitation wavelength was set at 460 nm, and emission was detected from 470 to 900 nm. The standard was 1 μM fluorescein in 1 mM NaOH/EtOH (ΦF = 0.92).

Fluorescence Titration Measurements. Fluorescence titration was performed according to the reported method with some modifications.[21] Briefly, the hRXRα-LBD protein solution was diluted from the stock solution with HEPES buffer (pH 7.9) containing 1% DMSO to a final concentration of 0.5 μM. Compound **7** was stocked in 20 mM DMSO and diluted (final concentration; 0.03125−4 μM) with HEPES buffer as required before use in the assay. The hRXRα-LBD protein solution was added to each concentration of the compound solution, and the mixture was incubated at room temperature for 2 h. The fluorescence spectrum of the complex of hRXRα-LBD with each complex was recorded in the wavelength range of 300−500 nm after excitation at 280 nm. The binding ratio was calculated as $[1 - F_{327nm}/F0_{327nm}]$ (at 327 nm) or $[F_{488nm}/F0_{488nm}]$ (at 488 nm). $F0$ is the fluorescence intensity in the absence of **7** at each wavelength, and F is the observed fluorescence intensity. The dissociation constant, Kd, was calculated by GraphPad Prism 8 software to fit the binding ratio as described elsewhere.[22]

*IC_{50} Determination of Test Compounds Using **7**.* The competitive binding assay using **7** was performed as described[14] with some modifications (see Figure S5). Black 384-well plates purchased from Griner were used (4 wells per sample). Solutions were prepared by the same method as described for the fluorescence titration measurements. To each well, 10 μL of hRXRα-LBD at 1 μM (final concentration: 0.5 μM), 5 μL of the sample at 4 times higher concentration than the final concentration, and 5 μL of 400 nM **7** (final concentration: 100 nM) were added. The mixture was incubated for 2 h at room temperature, and then the fluorescence intensity was measured at λ_{Ex} = 430 nm/λ_{Em} = 535 nm or λ_{Ex} = 485 nm/λ_{Em} = 535 nm with a TECAN infinite 200 Pro. The specific binding curve was obtained by subtraction of the fluorescence value for the hRXRα-LBD with a test compound in the absence of **7** from that in the presence of **7**. The specific equilibrium binding constant (Ki) was derived from the specific binding curve by fitting the data to a sigmoid equation using GraphPad Prism 8 software.

■ ASSOCIATED CONTENT

Supporting Information

The Supporting Information is available free of charge at https://pubs.acs.org/doi/10.1021/acs.jmedchem.0c01883.

Preparation of human RXRα-LBD, creation of human RXRα ligand-binding domain (LBD) coordinates,

https://dx.doi.org/10.1021/acs.jmedchem.0c01883
J. Med. Chem. 2021, 64, 861−870

coordinates for compounds (input files), creating the grid box, creating input files and log files of docking simulations, calculation of the Z' factor, statistical analysis, Schild analysis of **6** and **7** for hRXRα, transactivation of hRXR subtypes by **17** in the absence or presence of **7**, UV−vis absorbance and fluorescence spectra of fluorescein and **7**, relative fluorescence intensity data of 100 nM **7** in various solvents, chemical structure of CBTF-EE (**19**), binding assay protocol for rexinoids using **7** (λ_{Ex} = 430 nm/λ_{Em} = 535 nm), time course of Z' factors during the competitive binding assay using 100 nM **7** with 500 nM hRXRα-LBD, chemical structures of rexinoids in Figure 5B and natural ligands in Figure 5C, fluorescence binding assay using **7** (λ_{Ex} = 485 nm/λ_{Em} = 535 nm), Schild plot slopes for **6** and **7** against **17**, calculated *Ki* values obtained with **4**, **7**, and 9*cis*-RA, lists of PDB files, supporting movie legend, NMR spectra and HPLC charts (PDF)

Binding model of **7** (green stick model) in the antagonistic form with RXRα-LBD (PDB code: 3A9E) on AutoDock vina (MOV)

RXR_LBD 3A9E.pdb (chain A from pdb. 3A9E) (PDB)

Cpnd 5_mode1.pdb (mode 1 structure of NEt-SB (**5**) in RXR_LBD after docking) (PDB)

Cpnd 6_mode1.pdb (mode 1 structure of NEt-BA (**6**) in RXR_LBD after docking) (PDB)

Cpnd 6_mode2.pdb (mode 1 structure of NEt-BA (**6**) in RXR_LBD after docking) (PDB)

Cpnd 7_mode1.pdb (mode 1 structure of NEt-C343 (**7**) in RXR_LBD after docking) (PDB)

Cpnd 7_mode6.pdb (mode 6 structure of NEt-C343 (**7**) in RXR_LBD after docking) (PDB)

LG_3A9E.pdb (binding structure of LG100754 (**18**) "754" from pdb. 3A9E) (PDB)

Molecular formula strings and some data (CSV)

AUTHOR INFORMATION

Corresponding Author

Hiroki Kakuta − *Division of Pharmaceutical Sciences, Okayama University Graduate School of Medicine, Dentistry and Pharmaceutical Sciences, Kita-ku, Okayama 700-8530, Japan;* orcid.org/0000-0002-3633-8121; Phone: +81-(0)86-251-7963; Email: kakuta-h@okayama-u.ac.jp

Authors

Kayo Yukawa-Takamatsu − *Division of Pharmaceutical Sciences, Okayama University Graduate School of Medicine, Dentistry and Pharmaceutical Sciences, Kita-ku, Okayama 700-8530, Japan*

Yifei Wang − *Division of Pharmaceutical Sciences, Okayama University Graduate School of Medicine, Dentistry and Pharmaceutical Sciences, Kita-ku, Okayama 700-8530, Japan*

Masaki Watanabe − *Division of Pharmaceutical Sciences, Okayama University Graduate School of Medicine, Dentistry and Pharmaceutical Sciences, Kita-ku, Okayama 700-8530, Japan*

Yuta Takamura − *Division of Pharmaceutical Sciences, Okayama University Graduate School of Medicine, Dentistry and Pharmaceutical Sciences, Kita-ku, Okayama 700-8530, Japan*

Michiko Fujihara − *Division of Pharmaceutical Sciences, Okayama University Graduate School of Medicine, Dentistry and Pharmaceutical Sciences, Kita-ku, Okayama 700-8530, Japan; AIBIOS Co. Ltd., Tokyo 106-0032, Japan*

Mariko Nakamura-Nakayama − *Division of Pharmaceutical Sciences, Okayama University Graduate School of Medicine, Dentistry and Pharmaceutical Sciences, Kita-ku, Okayama 700-8530, Japan*

Shoya Yamada − *Division of Pharmaceutical Sciences, Okayama University Graduate School of Medicine, Dentistry and Pharmaceutical Sciences, Kita-ku, Okayama 700-8530, Japan; Research Fellowship Division, Japan Society for the Promotion of Science, Tokyo 102-8472, Japan*

Shota Kikuzawa − *Division of Pharmaceutical Sciences, Okayama University Graduate School of Medicine, Dentistry and Pharmaceutical Sciences, Kita-ku, Okayama 700-8530, Japan*

Makoto Makishima − *Division of Biochemistry, Department of Biomedical Sciences, Nihon University School of Medicine, Tokyo 173-8610, Japan;* orcid.org/0000-0002-4630-905X

Mayu Kawasaki − *Graduate School of Integrated Pharmaceutical and Nutritional Sciences, University of Shizuoka, Shizuoka 422-8526, Japan*

Sohei Ito − *Graduate School of Integrated Pharmaceutical and Nutritional Sciences, University of Shizuoka, Shizuoka 422-8526, Japan;* orcid.org/0000-0002-9937-3100

Shogo Nakano − *Graduate School of Integrated Pharmaceutical and Nutritional Sciences, University of Shizuoka, Shizuoka 422-8526, Japan;* orcid.org/0000-0002-6614-7158

Complete contact information is available at: https://pubs.acs.org/10.1021/acs.jmedchem.0c01883

Author Contributions

K.Y.-T. and H.K. conceived and designed the project. K.Y.-T., W.Y., and M.N.-N. synthesized the compounds. W.Y. performed NMR. M.W., Y.T., and S.K. performed MS analysis. W.Y., M.W., and S.K. performed HPLC. M.K. and S.N. produced hRXRα-LBD. M.F. performed reporter gene assays. M.W., Y.T., S.Y., and H.K. performed the RI binding assay. K.Y.-T., M.W., M.F., and H.K. analyzed the UV and fluorescence spectra. M.W., Y.T., and H.K. performed docking simulation. K.Y.-T. and M.F. performed fluorescence-based binding assay. All authors analyzed and discussed the data. The manuscript was written by K.Y.-T., M.W., and H.K.

Funding

This work was partially supported by Kobayashi Foundation (to H.K.), Okayama Foundation for Science and Technology (to H.K.), The Tokyo Biochemical Research Foundation (TBRF) (to H.K.), Grant-in-Aid from the Japan Society for the Promotion of Science (JSPS) (to S.Y.), JSPS KAKENHI Grant Numbers 16K18688, 18K14391 (to S.N.) and 17K06931(to S.I.), Kobayashi Foundation (to H.K.), and scholarship support from the Shoshisha Foundation (to Y.T.).

Notes

The authors declare the following competing financial interest(s): This research was partially performed in collaboration with AIBIOS Co., Ltd.. Michiko Fujihara was an employee of AIBOS. No other author reports any potential conflict of interest relevant to this article.

■ ACKNOWLEDGMENTS

The authors are grateful to the Division of Instrumental Analysis, Okayama University for the NMR and MS measurements. We are also grateful to Tecan and Fujifilm Wako Pure Chemical Corporation for supporting the TECAN infinite 200 Pro.

■ ABBREVIATIONS

Abs, absorption; Ac_2O, acetic anhydride; Arg321, arginine 321; B/F, bound-free; DHA, docosahexaenoic acid; DIEPA, *N*,*N*-diisopropylethylamine; DMF, *N*,*N*-dimethylformamide; DMSO, dimethyl sulfoxide; DTT, dithiothreitol; EDCI·HCl, *N*-(3-dimethylaminopropyl)-*N*′-ethyl carbodiimide hydrochloride; Em, emission; EPA, eicosapentaenoic acid; EtOH, ethanol; Ex, excitation; Fl, fluorescence; HOBt, 1-hydroxybenzotriazole; HPLC, high-performance liquid chromatography; hRXR, human RXR; LBD, ligand-binding domain; LBP, ligand-binding pocket; LXR, liver X receptor; MOMCl, methoxymethyl chloride; MS, mass spectrometry; NMR, nuclear magnetic resonance; Nurr1, nuclear receptor related 1 protein; PPAR, peroxisome proliferator activated receptor; q.y., quantitative yield; RAR, retinoic acid receptor; RI, radioisotope; r.t., room temperature; RXR, retinoid X receptor; SD, standard deviation; TBTCl, tributyltin chloride; TEA, triethylamine; TLC, thin-layer chromatography; TR, thyroid hormone receptor; TR-FRET, time-resolved fluorescence resonance energy transfer; Trp, tryptophan; UV, ultraviolet; VDR, vitamin D receptor

■ REFERENCES

(1) Esteva, F. J.; Glaspy, J.; Baidas, S.; Laufman, L.; Hutchins, L.; Dickler, M.; Tripathy, D.; Cohen, R.; DeMichele, A.; Yocum, R. C.; Osborne, C. K.; Hayes, D. F.; Hortobagyi, G. N.; Winer, E.; Demetri, G. D. Multicenter Phase II Study of Oral Bexarotene for Patients with Metastatic Breast Cancer. *J. Clin. Oncol.* **2003**, *21*, 999−1006.

(2) Cummings, J. L.; Zhong, K.; Kinney, J. W.; Heaney, C.; Moll-Tudla, J.; Joshi, A.; Pontecorvo, M.; Devous, M.; Tang, A.; Bena, J. Double-Blind, Placebo-Controlled, Proof-of-Concept Trial of Bexarotene Xin Moderate Alzheimer's Disease. *Alzheimer's Res. Ther.* **2016**, *8*, 4−9.

(3) McFarland, K.; Spalding, T. A.; Hubbard, D.; Ma, J. N.; Olsson, R.; Burstein, E. S. Low Dose Bexarotene Treatment Rescues Dopamine Neurons and Restores Behavioral Function in Models of Parkinson's Disease. *ACS Chem. Neurosci.* **2013**, *4*, 1430−1438.

(4) Evans, R. M.; Mangelsdorf, D. J. Nuclear Receptors, RXR, and the Big Bang. *Cell* **2014**, *157*, 255−266.

(5) Schierle, S.; Merk, D. Therapeutic Modulation of Retinoid X Receptors − SAR and Therapeutic Potential of RXR Ligands and Recent Patents. *Expert Opin. Ther. Pat.* **2019**, *29*, 605−621.

(6) Mukherjee, R.; Davies, P. J. A.; Crombie, D. L.; Bischoff, E. D.; Cesario, R. M.; Jow, L.; Hamann, L. G.; Boehm, M. F.; Mondon, C. E.; Nadzan, A. M.; Paterniti, J. R., Jr.; Heyman, R. A. Sensitization of Diabetic and Obese Mice to Insulin by Retinoid X Receptor Agonists. *Nature* **1997**, *386*, 407−410.

(7) Germain, P.; Chambon, P.; Eichele, G.; Evans, R. M.; Lazar, M. A.; Leid, M.; De Lera, A. R.; Lotan, R.; Mangelsdorf, D. J.; Gronemeyer, H. International Union of Pharmacology. LXIII. Retinoid X Receptors. *Pharmacol. Rev.* **2006**, *58*, 760−772.

(8) Takamatsu, K.; Takano, A.; Yakushiji, N.; Morohashi, K.; Morishita, K.; Matsuura, N.; Makishima, M.; Tai, A.; Sasaki, K.; Kakuta, H. The First Potent Subtype-Selective Retinoid X Receptor (RXR) Agonist Possessing a 3-Isopropoxy-4-Isopropylphenylamino Moiety, NEt-3IP (RXRα/β-Dual Agonist). *ChemMedChem* **2008**, *3*, 780−787.

(9) Pollinger, J.; Schierle, S.; Gellrich, L.; Ohrndorf, J.; Kaiser, A.; Heitel, P.; Chaikuad, A.; Knapp, S.; Merk, D. A Novel Biphenyl-Based Chemotype of Retinoid X Receptor Ligands Enables Subtype and Heterodimer Preferences. *ACS Med. Chem. Lett.* **2019**, *10*, 1346−1352.

(10) de Almeida, N. R.; Conda-Sheridan, M. A Review of the Molecular Design and Biological Activities of RXR Agonists. *Med. Res. Rev.* **2019**, *39*, 1372−1397.

(11) Pinaire, J. A.; Reifel-Miller, A. Therapeutic Potential of Retinoid X Receptor Modulators for the Treatment of the Metabolic Syndrome. *PPAR Res.* **2007**, *2007*, 94156.

(12) Sanders, M.; Chandraratna, R.; Marek, K.; Jennings, D. A Phase 1 Clinical Study of the Retinoid X Receptor (RXR) Selective Agonist IRX4204 in Patients with Early Parkinson's Disease (PD) (P2.342). *Neurology* **2016**, *86*, P2.342.

(13) Morishita, K.; Kakuta, H. Retinoid X Receptor Ligands with Anti-Type 2 Diabetic Activity. *Curr. Top. Med. Chem.* **2016**, *17*, 696−707.

(14) Yamada, S.; Kawasaki, M.; Fujihara, M.; Watanabe, M.; Takamura, Y.; Takioku, M.; Nishioka, H.; Takeuchi, Y.; Makishima, M.; Motoyama, T.; Ito, S.; Tokiwa, H.; Nakano, S.; Kakuta, H. Competitive Binding Assay with an Umbelliferone-Based Fluorescent Rexinoid for Retinoid X Receptor Ligand Screening. *J. Med. Chem.* **2019**, *62*, 8809−8818.

(15) Tomlinson, C. W. E.; Whiting, A. The Development of Methodologies for High-Throughput Retinoic Acid Binding Assays in Drug Discovery and Beyond. *Methods Enzymol.* **2020**, *637*, 539−560.

(16) Nakayama, M.; Yamada, S.; Ohsawa, F.; Ohta, Y.; Kawata, K.; Makishima, M.; Kakuta, H. Discovery of a Potent Retinoid X Receptor Antagonist Structurally Closely Related to RXR Agonist NEt-3IB. *ACS Med. Chem. Lett.* **2011**, *2*, 896−900.

(17) Yamada, S.; Takamura, Y.; Fujihara, M.; Kawasaki, M.; Ito, S.; Nakano, S.; Kakuta, H. Fluorescence Properties of Retinoid X Receptor Antagonist NEt-SB. *Bioorg. Med. Chem. Lett.* **2021**, *31*, 127666 DOI: 10.1016/j.bmcl.2020.127666.

(18) Gutierrez, J. A.; Falcone, R. D.; Lopez-Quintela, M. A.; Buceta, D.; Silber, J. J.; Correa, N. M. On the Investigation of the Droplet-Droplet Interactions of Sodium 1,4-Bis(2-Ethylhexyl) Sulfosuccinate Reverse Micelles upon Changing the External Solvent Composition and Their Impact on Gold Nanoparticle Synthesis. *Eur. J. Inorg. Chem.* **2014**, *2014*, 2095−2102.

(19) Reynolds, G. A.; Drexhage, K. H. New Coumarin Dyes with Rigidized Structure for Flashlamp-Pumped Dye Lasers. *Opt. Commun.* **1975**, *13*, 222−225.

(20) Van Gompel, J.; Schuster, G. B. Chemiluminescence of Organic Peroxides: Intramolecular Electron-Exchange Luminescence from a Secondary Perester. *J. Org. Chem.* **1987**, *52*, 1465−1468.

(21) Yung-Chi, C.; Prusoff, W. H. Relationship between the Inhibition Constant (KI) and the Concentration of Inhibitor Which Causes 50 per Cent Inhibition (I50) of an Enzymatic Reaction. *Biochem. Pharmacol.* **1973**, *22*, 3099−3108.

(22) Cheng, L.; Norris, A. W.; Tate, B. F.; Rosenberger, M.; Grippo, J. F.; Li, E. Characterization of the Ligand Binding Domain of Human Retinoid X Receptor α Expressed in Escherichia Coli. *J. Biol. Chem.* **1994**, *269*, 18662−18667.

(23) Birdsall, B.; King, R. W.; Wheeler, M. R.; Lewis, C. A., Jr.; Goode, S. R.; Dunlap, R. B.; Roberts, G. C. K. Correction for Light Absorption in Fluorescence Studies of Protein-Ligand Interactions. *Anal. Biochem.* **1983**, *132*, 353−361.

(24) Zhang, X. F.; Zhang, J.; Liu, L. Fluorescence Properties of Twenty Fluorescein Derivatives: Lifetime, Quantum Yield, Absorption and Emission Spectra. *J. Fluoresc.* **2014**, *24*, 819−826.

(25) Magde, D.; Wong, R.; Seybold, P. G. Fluorescence Quantum Yields and Their Relation to Lifetimes of Rhodamine 6G and Fluorescein in Nine Solvents: Improved Absolute Standards for Quantum Yields. *Photochem. Photobiol.* **2002**, *75*, 327−334.

(26) Satpathi, S.; Sappati, S.; Das, K.; Hazra, P. Structural Characteristics Requisite for the Ligand- Based Selective Detection of i-Motif DNA. *Org. Biomol. Chem.* **2019**, *17*, 5392−5399.

(27) Riter, R. E.; Undiks, E. P.; Levinger, N. E. Impact of Counterion on Water Motion in Aerosol OT Reverse Micelles. *J. Am. Chem. Soc.* **1998**, *120*, 6062−6067.
(28) Jiménez-Sánchez, A.; Lei, E. K.; Kelley, S. O. A Multifunctional Chemical Probe for the Measurement of Local Micropolarity and Microviscosity in Mitochondria. *Angew. Chem., Int. Ed.* **2018**, *57*, 8891−8895.
(29) Moreira, L. M.; De Melo, M. M.; Martins, P. A.; Lyon, J. P.; Romani, A. P.; Codognoto, L.; dos Santos, S. C.; De Oliveira, H. P. M. Photophysical Properties of Coumarin Compounds in Neat and Binary Solvent Mixtures: Evaluation and Correlation between Solvatochromism and Solvent Polarity Parameters. *J. Braz. Chem. Soc.* **2014**, *25*, 873−881.
(30) Cigáň, M.; Donovalová, J.; Szöcs, V.; Gašpar, J.; Jakusová, K.; Gáplovský, A. 7-(Dimethylamino)Coumarin-3-Carbaldehyde and Its Phenylsemicarbazone: TICT Excited State Modulation, Fluorescent H-Aggregates, and Preferential Solvation. *J. Phys. Chem. A* **2013**, *117*, 4870−4883.
(31) El Seoud, O. A. Understanding Solvation. *Pure Appl. Chem.* **2009**, *81*, 697−707.
(32) Morris, G. M.; Huey, R.; Lindstrom, W.; Sanner, M. F.; Belew, R. K.; Goodsell, D. S.; Olson, A. J. AutoDock4 and AutoDockTools4: Automated Docking with Selective Receptor Flexibility. *J. Comput. Chem.* **2009**, *30*, 2785−2791.
(33) Sato, Y.; Ramalanjaona, N.; Huet, T.; Potier, N.; Osz, J.; Antony, P.; Peluso-Iltis, C.; Poussin-Courmontagne, P.; Ennifar, E.; Mély, Y.; Dejaegere, A.; Moras, D.; Rochel, N. The "Phantom Effect" of the Rexinoid LG100754: Structural and Functional Insights. *PLoS One* **2010**, *5*, No. e15119.
(34) Trott, O.; Olson, A. J. Autodock Vina: Improving the Speed and Accuracy of Docking. *J. Comput. Chem.* **2010**, *31*, 455−461.
(35) Watanabe, M.; Fujihara, M.; Motoyama, T.; Kawasaki, M.; Yamada, S.; Takamura, Y.; Ito, S.; Makishima, M.; Nakano, S.; Kakuta, H. Discovery of a "Gatekeeper" Antagonist that Blocks Entry Pathway to Retinoid X Receptors without Allosteric Ligand Inhibition in Permissive RXR Heterodimers. *J. Med. Chem.* in press DOI: 10.1021/acs.jmedchem.0c01354.
(36) Lengqvist, J.; Mata de Urquiza, A.; Bergman, A. C.; Willson, T. M.; Sjövall, J.; Perlmann, T.; Griffiths, W. J. Polyunsaturated Fatty Acids Including Docosahexaenoic and Arachidonic Acid Bind to the Retinoid X Receptor α Ligand-Binding Domain. *Mol. Cell. Proteomics* **2004**, *3*, 692−703.
(37) Stewart, J. J. P. Optimization of Parameters for Semiempirical Methods II. Applications. *J. Comput. Chem.* **1989**, *10*, 221−264.
(38) Kakuta, H.; Yakushiji, N.; Shinozaki, R.; Ohsawa, F.; Yamada, S.; Ohta, Y.; Kawata, K.; Nakayama, M.; Hagaya, M.; Fujiwara, C.; Makishima, M.; Uno, S.; Tai, A.; Maehara, A.; Nakayama, M.; Oohashi, T.; Yasui, H.; Yoshikawa, Y. RXR Partial Agonist CBt-PMN Exerts Therapeutic Effects on Type 2 Diabetes without the Side Effects of RXR Full Agonists. *ACS Med. Chem. Lett.* **2012**, *3*, 427−432.
(39) Allenby, G.; Bocquel, M. T.; Saunders, M.; Kazmer, S.; Speck, J.; Rosenberger, M.; Lovey, A.; Kastner, P.; Grippo, J. F.; Chambon, P. Retinoic Acid Receptors and Retinoid X Receptors: Interactions with Endogenous Retinoic Acids. *Proc. Natl. Acad. Sci. U. S. A.* **1993**, *90*, 30−34.
(40) Levin, A. A.; Sturzenbecker, L. J.; Kazmer, S.; Bosakowski, T.; Huselton, C.; Allenby, G.; Speck, J.; Ratzeisen, C.; Rosenberger, M.; Lovey, A.; Grippo, J. F. 9-*Cis* Retinoic Acid Stereoisomer Binds and Activates the Nuclear Receptor RXRα. *Nature* **1992**, *355*, 359−361.

https://dx.doi.org/10.1021/acs.jmedchem.0c01883
J. Med. Chem. 2021, 64, 861−870